Optimal Trajectory and En-Route Contingency Planning for Urban Air Mobility Considering Battery Energy Levels

Seulki Kim *, Caleb Harris †, Cedric Y. Justin ‡, and Dimitri Mavris §
Georgia Institute of Technology, Atlanta, GA 30332, USA

Urban Air Mobility (UAM) is an electric propelled, vertical takeoff and landing (eVTOL) aircraft envisioned for transporting passengers and goods within metropolitan areas. Planning UAM flights will not be easy as unexpected wind turbulence from high-altitude structures may impact the vehicles operating at a low altitude. Furthermore, considering the short travel time of the UAM, smart and safe decision-making will be challenging, particularly in off-nominal situations that force the aircraft to divert to an alternate destination instead of landing at the initially planned destination. To overcome these challenges, this research proposes automated pre-flight and in-flight contingency planning systems to assist in both normal and irregular UAM operations. A planner in the pre-flight planning system optimizes an aerial trajectory between the scheduled origin and destination, avoiding restricted high-level structures and estimating energy levels. In the contingency planning system, an in-flight replanner produces several optimal trajectories from where the diversion is declared to each alternate destination candidate. A diversion decision-making tool then scores a list of candidates and selects the best site for diversion. Real-world operational scenarios in the city of Miami are presented to demonstrate the capability of the proposed framework.

I. Nomenclature

Sets

$\mathcal{T}$	Set of discrete time steps, $t \in \{0, \ldots, N_T\}$
$\mathcal{T}^{-1}$	Set of discrete time steps except for last time interval, $t \in \{0, \ldots, N_T - 1\}$
$\mathcal{M}$	Set of m-sided polygons to approximate a circle, $m \in \{1, \ldots, N_M\}$
$\mathcal{S}$	Set of restricted airspace, $s \in \{1, \ldots, N_S\}$
$\mathcal{D}$	Set of alternate destinations, $i \in \{1, \ldots, N_D\}$

Continuous Decision Variables

(x_t, y_t)	Position of aircraft at time step t in x- and y-axes, respectively
(v_{x_t}, v_{y_t})	Velocity of aircraft at time step t in x and y-axes, respectively
(a_{x_t}, a_{y_t})	Acceleration of aircraft at time step t in x and y-axes, respectively

Binary Decision Variables

f_t	Binary indicators whether aircraft takes off at time step t
e_t	Binary indicators whether aircraft is airborne at time step t
d_t	Binary indicators whether aircraft is arrived to destination at time step t
n_{tsk}	Binary indicators whether aircraft intrudes into the sth restricted area in the kth direction of $+x$, $-x$, $+y$, $-y$ at time step t
δ_i	Binary indicators whether ith reachable alternate destination is selected

Parameters

*Graduate Research Assistant, Aerospace Systems Design Laboratory, School of Aerospace Engineering, AIAA Student Member
†Graduate Research Assistant, Aerospace Systems Design Laboratory, School of Aerospace Engineering, AIAA Student Member
‡Research Engineer II, Aerospace Systems Design Laboratory, School of Aerospace Engineering, and AIAA Member
§S.P. Langley NIA Distinguished Regents Professor and Director of Aerospace Systems Design Laboratory, School of Aerospace Engineering, AIAA Fellow

N_T	Number of discrete time
N_S	Number of restricted areas
N_M	Number of linear inequalities to approximate a circle
N_D	Number of reachable alternate destination candidates
Δt	Discrete time interval
t_{dep}	Departure time that aircraft plans to take off
(x^I, y^I)	Position of origin that aircraft is scheduled to take off in $x-$ and $y-$axes, respectively
(x^F, y^F)	Position of destination that aircraft is landed at in $x-$ and $y-$axes, respectively
$V_{\max}$	Maximum velocity
$a_{\max}$	Maximum acceleration
R	Sufficiently large number
ρ	Air density
W	Weight of vehicle
A	Total rotor disc areas
DL	Disk loading, $DL = W/A$
v_i	Induced velocity
v_h	Hover velocity
ROC	Rate of climb
L/D	Lift-to-drag
$\eta_{\text{hover}}, \eta_{\text{climb}}, \eta_{\text{cruise}}$	Hover, climb, and cruise efficiency factors, respectively
μ_{total}	Total efficiency factor
P	Power required
E	Energy required

II. Introduction

TECHNOLOGICAL advancements in automation, distributed electric propulsion, and electricity storage have spurred significant interest in and enabled the emergence of a new aerial transportation concept called Urban Air Mobility (UAM). Compared to traditional helicopters, electric propelled, vertical takeoff and landing (eVTOL) UAM vehicles are envisioned to offer faster, safer, and more sustainable transport of passengers and cargo over short distances and at low altitudes. It is anticipated that early-term UAM may initiate services with a limited number of scheduled flights along with pre-defined airspace structures (e.g., air corridor, sky-lane, etc.). Applications may be restricted to delivering goods or operating airport shuttles until the technical feasibility and economic viability are demonstrated [1, 2]. As onboard technologies (e.g., Detect-and-Avoid, navigation precision, etc.) and regulations mature, long-term air operations may deliver on-demand air taxi services, allowing passengers to take a ride whenever and wherever they desire [1, 3–5]. Some studies [6, 7] also expect that future operations may leverage operator-preferred aerial trajectories, i.e., free-flight, as long as their flight plans are generated, deconflicted from previously filled plans, and authorized by the provider of services for UAM (PSU), which is an organization that provides urban air traffic management comparable to the current air traffic controller (ATC).

With the anticipation of high-density UAM operations in the future, urban airspace will become increasingly crowded and complex. To effectively manage air traffic, flight planning will be an essential component in UAM operations, just as in commercial aviation [8, 9]. Flight planning is the process of producing trajectories with estimated times of departure and arrival, energy requirements, and potential alternate airports. The flight trajectory represents an aerial route between departure and arrival locations that considers velocity changes over time, avoids restricted airspace (i.e., no-fly zones), and safely separates airspace participants. Flight planning generally consists of pre-flight planning and potentially in-flight replanning. Pre-flight planning is performed to generate an initial plan before departure, while inflight replanning involves modification of the original plan in response to unexpected circumstances (e.g., disruption at the original airport, medical emergency, adverse weather, etc.) Planning UAM flights will be more challenging due to operations at low altitudes over congested cities. The UAM may encounter more restricted airspace than commercial flights operating at high altitudes. For example, aircraft should detour high-altitude structures in metropolitan areas (e.g., high-rise buildings, tower cranes, communication towers, etc.) because urban canyons or even a single structure can make unpredictable wind turbulence, thereby causing instability and loss of control of the vehicles [10, 11] even if they fly over the structures. Furthermore, eVTOL vehicles necessitate evaluating battery energy consumption and energy state required to reach the destination instead of estimating fuel consumption that the traditional flight plan has

considered. Therefore, a new flight planning system suitable for UAM operations must be introduced to avoid restricted high-level structures and estimate battery energy consumption and energy state.

Safe and efficient initial flight plans are generated through pre-flight planning using the most up-to-date information; however, they are not always followed because of dynamic and unforeseen nature events, requiring modification of the trajectory in the air. More importantly, an aircraft often confronts unfavorable circumstances that fail to land at its initially planned destination. There are two types of responses to such circumstances. The first one is an emergency landing, where the aircraft must land as quickly as possible, which may result from a critical system malfunction or failure. The second is a contingency diversion, where the aircraft operates normally but must divert to an alternate destination due to deteriorating weather conditions, an energy shortage, or a medical emergency. The latter is the focus of this research. The diversion procedure requires that the flight crew considers many elements. The flight crew needs to make a decision regarding where to divert and which trajectory to use while estimating heading, ground speed, arrival time, and energy consumption to the diversion airport. In the context of UAM operations, the diversion decision-making will be challenging because flight crews will have little time to consider all these aspects. For this reason, there is a need for decision support, and an automated in-flight contingency planning system may need to be developed to assist flight crews.

There have been significant efforts to develop flight planning tools in recent years. For example, Tang et al. [8] proposed a flight planning system that constructs a route network in low-altitude airspace using the visibility graph and produces conflict-free trajectories in the network. Although the paper successfully demonstrated the proposed system in managing high-density UAM flights in the constructed network, it assumes constant airspeed in all flights instead of optimizing them and does not consider the battery energy consumed for each origin-destination trip. Zhu and Wei [9] presented a pre-departure conflict-free trajectory planning with the dynamic geofence concept, which is a moving volume surrounding an aircraft to reserve airspace. However, the trajectory planning suggested in the paper lacks consideration for the avoidance of restricted airspace. Regarding the contingency planning to address irregular aircraft operations, Ayhan et al. [12] proposed a preflight contingency planning system that guides fixed-wing unmanned aerial vehicles to safely land at an emergency landing site during a complete loss of thrust situation. The shortcoming of this planning is that the aircraft will not be flexible in responding to unexpected off-nominal situations that might happen during the flight unless such situations are entirely predicted and prepared before the flight initiates.

To fill the gaps identified in previous literature, this research endeavors to develop an automated framework with two main systems of pre-flight planning and contingency planning. The pre-flight planning system consists of a planner leveraged for the UAM normal operations. The planner is constructed using a mixed-integer linear programming (MILP) approach to optimize an initial trajectory that avoids restricted areas and tracks the battery energy state from the origin to the planned destination. The contingency planning system composes an in-flight replanner and a diversion decision-making tool and is utilized when a diversion is declared due to any off-nominal situations. The in-flight planner uses MILP to generate optimal trajectories from where the diversion is declared to each reachable alternate destination candidate. The decision support tool is developed using integer linear programming (ILP) to select the best diversion destination from a list of candidates. The proposed framework is applied to real-world operational scenarios in the city of Miami to demonstrate the capability of the framework.

The remainder of the paper is structured as follows. Section III provides an overview of the proposed framework. Section IV explains how mathematical modeling has been done for the trajectory optimization using MILP and the diversion decision-making using ILP. Section V presents the application of the framework to three operational scenarios in the city of Miami with results and discussion.

III. Proposed Framework

This section proposes an automated framework that consists of two planning systems—pre-flight and contingency planning. Pre-flight planning includes a planner to optimize an aerial trajectory from the origin to the scheduled destination. Contingency planning comprises two subsystems, an in-flight replanner and a diversion decision-making tool. The former determines several optimal trajectories from a contingency point where diversion is declared to each reachable alternate landing site. The latter ranks the candidate landing sites based on a scoring function and then returns the best site for the UAM to be able to divert successfully.

Figure 1 illustrates an overall flowchart of the proposed framework. The pre-flight planner is first executed to produce an initial flight plan before departure. Once the PSU approves the plan by checking deconfliction and separation against previously filled plans, UAM initiates the operation. If the vehicle is able to complete the original plan, it finishes the flight by landing at the scheduled destination. If any off-nominal situation arises, the contingency planning

system is implemented. In such a system, the in-flight replanner generates multiple trajectories to each of the reachable alternate destinations, then the diversion decision support tool prioritizes them and returns the best option for an in-flight diversion. The updated flight plan is submitted to and re-approved by PSU if the new plan ensures safe operation without violating other flight plans. Lastly, the UAM successfully lands at the best diversion landing site. Further details with respect to each system are provided in Sections III.A and III.B.

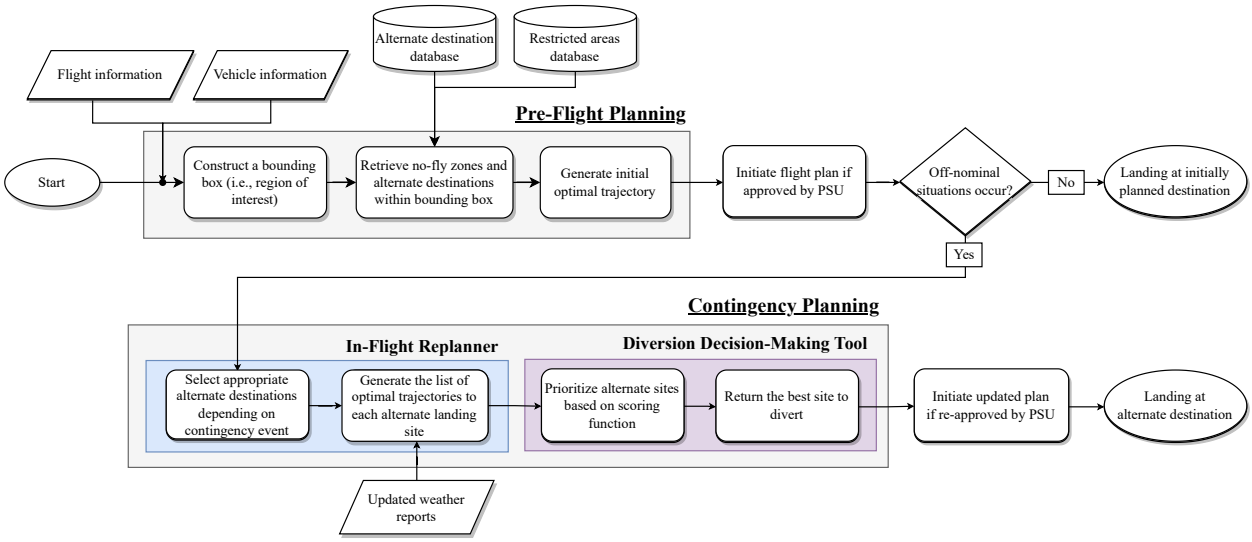

Fig. 1 Flowchart of the proposed framework

A. Pre-Flight Planning

1. Assumptions

The pre-flight planning system relies on the following assumptions: 1) only eVTOL aircraft are considered; 2) two-dimensional flight is considered. Once the vehicle reaches a cruise altitude, it maintains the same level until descent begins around the destination; 3) only the cruise segment is optimized along the trajectory, while the other segments, such as taxi, takeoff, climb, descent, and landing, are predefined with the fixed time; 4) all destinations have the same elevation.

2. Workflow of Planning System

Before the UAM initiates its operation, the pre-flight planner collects flight information, including flight schedules (origin and destination, and departure time), weather reports (wind velocity and direction, and hazardous weather conditions and locations), and no-fly zones (prohibited and restricted areas, and high-altitude structures). It also collects what type of UAM vehicles (vectored thrust, lift and cruise, and multicopter) and performance specifications (maximum take-off and weight, total battery energy, cruise speed, etc.) will be operated. Once all information regarding the flight operation and the vehicle is obtained, the planner sets a rectangular bounding box, namely a region of interest, by enclosing departure and arrival locations. Setting the region of interest can expedite computational time in optimization by excluding unnecessary regions that aircraft might not explore in operation. Within the bounding box, restricted areas and alternate landing site candidates are identified and retrieved from databases. Finally, the planner optimizes an initial trajectory with the objective of minimum travel time between the scheduled origin and destination, avoiding no-fly zones and tracking the consumed battery energy level.

3. Selection of eVTOL Vehicle

The Electric VTOL News website published by the Vertical Flight Society (VFS) provides a comprehensive directory for diverse types of eVTOL vehicles. According to the VFS, as of April 22, 2022, more than 500 UAM eVTOL concepts and designs have been proposed by major aircraft manufacturers, startups, innovators, and inventors [13]. The main

categories of eVTOL vehicles are vectored thrust, lift and cruise, and wingless multicopters. The vectored thrusts use any of their thrusters for both lift and cruise by adjusting the thrust vector to the desired direction. The lift and cruise aircraft have two sets of independent thrusters, one set for vertical lift and another set for the cruise, without any thrust vectoring. Lastly, the wingless muticopter vehicles utilize their thrusters to generate lift for vertical and horizontal flights. This work chooses vectored thrust eVTOLs for simulation. Joby S4 is one of the representatives of the vectored thrust vehicles (cruise speed of 322 km/h, range of 241 km, total battery energy of 180 kWh, etc.) and selected for simulation in this study. The detailed vehicle specification of Joby S4 can be found in [14, 15].

4. Mission Profile for UAM Operations

The general UAM mission profile comprises the following flight segments: taxi, hover, vertical take-off, climb, cruise, descent, vertical landing, hover, and taxi back. Specific to vectored thrust eVTOLs, the mission can be further extended by including transition segments as this type of vehicle configuration is changed from vertical (take-off/landing) to horizontal (cruise) flight and vice versa. The mission profile for vectored thrust eVTOL aircraft is illustrated in Figure 2.

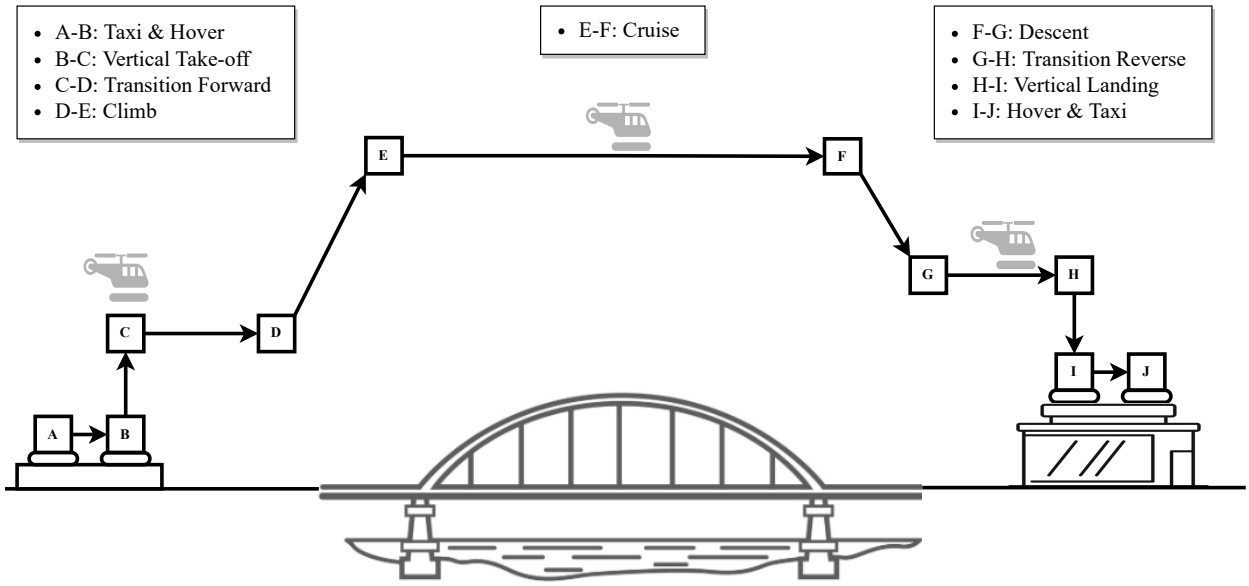

Fig. 2 Mission profile for vectored thrust eVTOL vehicles

5. Battery Energy Consumption Modeling

Trajectory planning for eVTOL vehicles has proved difficult because of the diversity and complexity of vehicle performance and operations. In particular, solving for the power available, the power required, and powertrain dynamics is not trivial when inputs are required from aerodynamic, propulsion, and control tasks. Furthermore, to find a feasible or even optimal solution, one must provide many assumptions about the vehicle design and flight profile. This is detailed and demonstrated in [16] where a 6-DOF aircraft dynamics model is integrated with a nonlinear powertrain model to evaluate the energy metrics along predefined and optimized trajectories. The computational time and number of parameters constrain the trade studies and exploratory analysis that needs to be done to evaluate en-route diversion decisions. Investigations into the modeling of the powertrain and integrated eVTOL vehicles can be seen in [17], and an alternative data-driven method for energy risk assessment is seen in [18].

Current UAM companies and academic research have sought to examine a wide range of scenarios using simplified models to gain insight into trends and trade studies in the complicated trade space for eVTOL system and system of systems. For example, Bruhl et al. [19] formulated a strategy for calculating power, energy, and ultimately range predictions for several types of eVTOL vehicles, such as vectored thrust, lift+cruise, and multicopter designs. A more

detailed breakdown of the equations for power usage is found in [20].

This paper defines a point-mass model aircraft and simplifies assumptions for flight segments of eVTOL vehicles. Table 1 describes the equations for the power calculations with assumptions made for each flight segment, in which more detail can be seen in [19]. The vehicle definition of the vectored thrust eVTOL is now constrained to the parameters seen here. The weight of the vehicle, W, and the disk loading, $DL = W/A$, are key parameters in hover performance with the remaining performance embedded in the efficiency factor, η_{hover}. Vertical take-off and landing require the additional power to fly vertically, which is calculated using momentum theory [21]. A ratio for the induced velocity, v_i, and hover velocity, v_h, can be formed and simplified to the equation shown here. The only remaining parameters are the desired rate-of-climb, ROC, during climb and takeoff and rate-of-descent, ROD, during descent and landing.

Table 1 Summary of equations for eVTOL power calculation for each flight segment

Flight Segment	Assumption	Equation
Hover	Vertical thrust equals weight Hover efficiency term accounts for profile drag and more	$P_{\text{hover}} = \frac{W}{\eta_{\text{hover}}}\sqrt{\frac{DL}{\rho}}$
Cruise	Thrust equals drag, weight equals lift Free-body diagram of point mass model	$P_{\text{cruise}} = \frac{W\, v_{\text{cruise}}}{(L/D)_{\text{cruise}}\,\eta_{\text{cruise}}}$
Vertical Take-off/Landing	Momentum Theory [21]	$P_{to} = P_{\text{hover}}\left(\frac{ROC_{to}}{2v_h} + \sqrt{\frac{ROC_{to}}{2v_h}^2 + 1}\right)$
Climb/Descent	Small angle assumption so lift equals weight Thrust equals drag and component of weight, constant rate-of-climb	$P_{\text{climb}} = \frac{W}{\eta_{\text{climb}}}\left(ROC_{cl} + \frac{v_{climb}}{(L/D)_{\text{climb}}}\right)$
Transition	Assume level transition as in [20] and velocity at end of maneuver	$P_{\text{trans}} = P_{\text{induced}} + P_{\text{profile}} + P_{\text{drag}}$

The climb and descent phases have a few simplifying assumptions to organize the equation with key parameters. A small angle assumption and constant rate-of-climb and rate-of-descent constraints are added, allowing the power to be determined using weight, the rate-of-climb or rate-of-descent, velocity, and lift-to-drag, L/D. The use of the lift-to-drag parameter is an example of the level of parameterization desired by this model, where this single term could evaluate a range of vehicle aerodynamics. Generally, the lift-to-drag is inversely proportional to the energy required for a given flight path. An additional efficiency factor, η_{climb} is added for any additional losses not modeled.

The transition model is the most difficult to model and requires additional assumptions. A level transition with a constant velocity equal to the velocity at the end of the transition maneuver is assumed. This allows for a simple formulation relying on momentum theory and force balancing. The traditional rotorcraft power organization is used, with total power for transition computed as a combination of the three power categories: induced power from the induced velocity through the rotor, profile power from the rotor motion, and drag power from the body of the vehicle moving through the air.

Cruise performance is of primary interest for the power calculation for different trajectories since each trajectory generally requires the same takeoff and landing phases. The cruise segment is defined as a force balance between lift and weight, and thrust and drag. Thus, the flight condition is abstracted to only three flight parameters: cruise velocity v_{cruise}, lift-to-drag, and efficiency such that

$$P_{\text{cruise}} = \frac{W \cdot v_{\text{cruise}}}{(L/D)_{\text{cruise}} \cdot \eta_{\text{cruise}}}.$$

Over each of the flight segments, the energy used is simply the power multiplied by the amount of time. For n flight segments, the total energy is formulated by a summation as

$$E_{\text{total}} = \sum_{i=1}^{n} P_i t_i.$$

The battery depletion is modeled with the total efficiency and the depth of discharge. The total efficiency is a product of several efficiency factors from the battery, electric motors, controllers, gearbox, etc. The depth of discharge is the limit of the extractable energy within the battery. The power drawn from the battery is then defined as the ratio of the power required divided by the total efficiency factor as

$$P_{\text{battery}} = \frac{P_{\text{aircraft}}}{\mu_{\text{total}}}.$$

Lastly, the state of charge (SOC) of the battery is a useful parameter for tracking the energy state of an electric propulsion system. For this work, it is assumed to be a linear model of the known extractable energy within the system and is normalized between 0 and 100%, defined as

$$SOC_{\text{battery,used}} = \frac{E_{\text{total}} - E_{\text{used}}}{E_{\text{total}}} \times 100\%. \tag{1}$$

Although this is a simplification, it is acceptable for the current experiments and could be improved in future work. Figure 3 highlights altitude and battery SOC changes simulated using the SOC metric over the course of a mission defined in Section III.A.4. The battery SOC limit, SOC_{limit}, is generally set to 20-30% of the overall capacity of the battery to prevent damage to the battery (aging) and preserve longevity [22]. This research sets the SOC limit to 20% and utilizes the parameter values presented in [19] for the power and energy calculations of the vectored thrust eVTOLs.

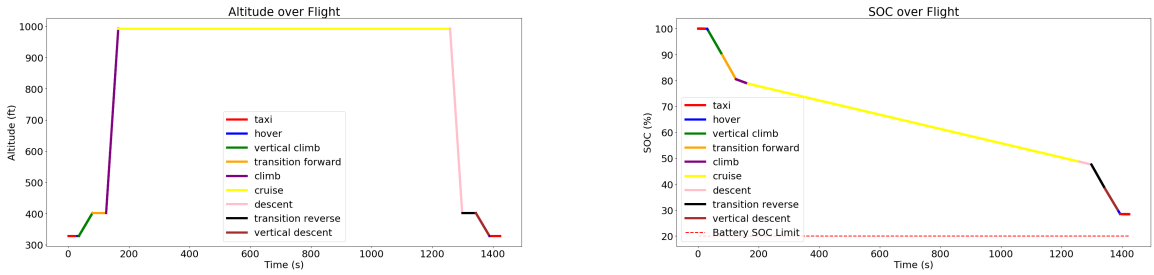

(a) Altitude change over mission profile

(b) State of charge change over mission profile

Fig. 3 Demonstration of battery energy consumption model

B. Contingency Planning

1. Assumptions

Two assumptions are made about the contingency planning system: 1) all alternate destinations have landing facilities, such as touchdown and liftoff area (TLOF), final-approach and take-off area (FATO), and safety area that can accommodate any eVTOL vehicles; 2) alternate landing sites have sufficient capacity to accommodate unplanned diversions.

2. Off-nominal Scenarios

This research defines two contingency situations that result in deviations from an initial flight plan and rerouting to the diversion destination. The first scenario is the case where an aircraft would not be able to land at an intended destination because of disruptions from arrival delays or accidents (e.g., fire, explosions, etc.). In this scenario, it is worth mentioning that once the aircraft has landed at one of the possible alternate destinations, passengers would have to return to the original aerodrome by taking ground transportation to reach their final destinations eventually. Hence, this case necessitates considering not only UAM flight time to reach the diversion landing site but also the recovery time that it takes for passengers to head back to the planned destination. The second scenario is the case of an in-flight medical emergency where an onboard passenger may experience a severe health problem (e.g., fainting, heart attack, nausea, etc.) during flight. In such a case, a pilot decides to either continue the planned flight or declare diversion based on the condition of the patients. If the situation is urgent, the pilot looks for the closest hospital equipped with an adequate emergency facility and changes the route to reach there. As the primary objective is immediate care, it is necessary to transport the patient in critical condition to the hospital as quickly as possible; that is, this case requires the least UAM travel time.

3. Workflow of Planning System

The contingency planning system is executed as soon as the continuation of the flight to the original destination is deemed impracticable. In the system, the in-flight replanner first extracts the appropriate alternate destination candidates

along with the off-nominal event type, described in Section III.B.2. For instance, heliports and hospitals are selected as candidates in cases of disruption at the original destination and medical emergency, respectively. Next, monitoring changes in the weather conditions, the in-flight replanner produces multiple optimal trajectories from the contingency location to each of the selected candidates to make a reasonable estimate of heading, ground speed, arrival time, and battery energy consumption to the candidates. It is worth mentioning that the replanner eliminates some of the landing sites from a list of candidates where reachability is not satisfied, given the remaining battery state. As the next step in the system, the diversion decision support tool defines a scoring function, depending on the off-nominal event, to evaluate the priority of candidates. In the case of a disruption at the original destination, the scoring function is created by combining travel time from UAM flight and passenger recovery time from ground transportation. For the medical emergency case, the function is formed only with the flight time. The decision tool then prioritizes candidates with the smallest function value and returns the best site to divert. Figure 4 notionally illustrates how the diversion decision tool selects the best alternate destination in the two contingency situations.

(a) Heliport 2 is selected with the least sum of flight and passenger recovery time in the first scenario of original destination disruption

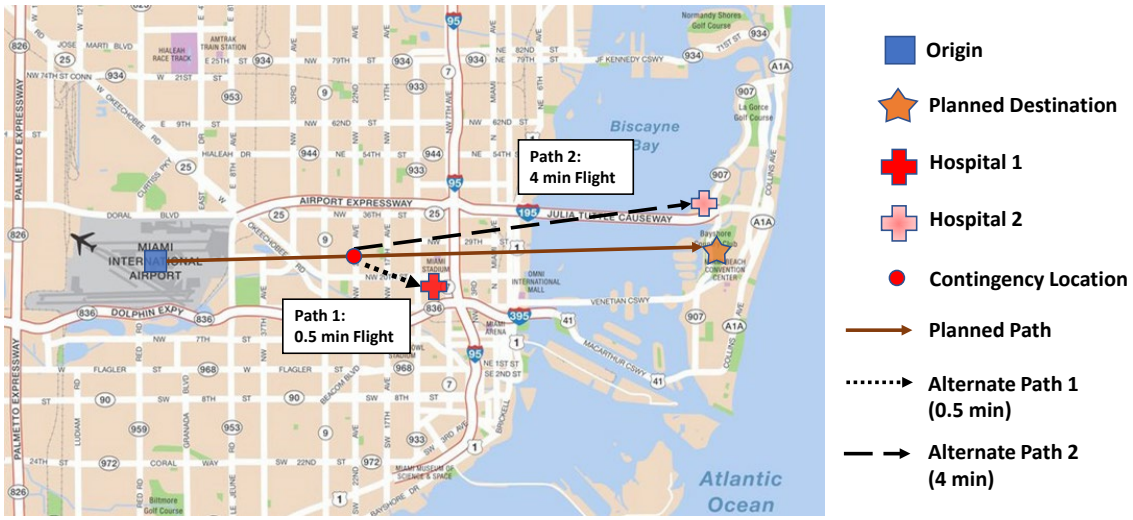

(b) Hospital 1 is selected with the least flight time in the second scenario of an in-flight medical emergency

Fig. 4 The selection process of alternate landing site and associated trajectory by diversion decision-making tool in two off-nominal scenarios

4. Passenger Recovery Time Evaluation to Original Destination

This research leverages the Microsoft Bing Map application programming interface (API) to evaluate the recovery time for passengers to return to their original destination by taking ground transportation. The Route API in the Bing Map provides the estimated travel time and distance for any pair of origin and destination locations with predictive traffic data [23]. The distance and duration are calculated based on the best route, which is determined by transport modes (i.e., walking, driving, and using transit). Estimated duration also varies depending on travel start time as road traffic conditions change with time. Listing 1 shows an example of the estimated travel duration result with traffic information from the Route API. The output shows that traveling between start and end locations, highlighted by yellow, by driving takes 792 and 1,186 seconds without and with consideration of traffic volume, highlighted by green. This research assumes that every passenger that diverts to an alternate destination would travel back to the original destination using a ground vehicle.


```
{'bbox': [25.787739, -80.211017, 25.814061, -80.138769],
 'distanceUnit': 'Kilometer',
 'durationUnit': 'Second',
 'routeLegs':
    [{'actualEnd': 'type': 'Point', 'coordinates': [25.792893, -80.211017],
     'actualStart': 'type': 'Point', 'coordinates': [25.814061, -80.141671],
     'cost': 0,
     'description': 'FL-934, I-95 S',
     'endTime': '/Date(1647175153000-0800)/',
     'startTime': '/Date(1647172800000-0800)/',
     'routeRegion': 'WWMX'}],
 'trafficCongestion': 'Medium',
 'trafficDataUsed': 'FlowAndClosure',
 'travelDistance': 11.522,
 'travelDuration': 792,
 'travelDurationTraffic': 1186,
 'travelMode': 'Driving'}
```


Listing 1 Estimated travel time by driving with predictive traffic volume

IV. Mathematical Modeling

A. MILP-based Trajectory Optimization

The pre-flight planner and in-flight replanner attempt to find the optimal trajectory with the goal of minimizing flight time, avoiding restricted areas, and evaluating the consumption of battery energy for the mission. This research utilizes discrete optimization in the form of Mixed Integer Linear Programming (MILP). The MILP forces all objectives and constraints to be linear and can be a combination of continuous and discrete variables. Due to the requirement of linearity, the non-linear vehicle dynamics and the quadratic form of the maximum velocity and acceleration limits are linearly approximated. In addition, constraints, such as obstacle avoidance and destination arrival, are linearly formulated in the optimization. The mathematical modeling described below builds upon well-known literature [24, 25].

In the trajectory optimization, the mathematical formulations and their associated decision variables are defined over the finite time horizon T. The time horizon is discretized by a given number of time steps N_T such that $T = N_T \Delta t$, where Δt is a fixed time step length. Let $\mathcal{T} = \{0, \ldots, N_T\}$ and $\mathcal{T}^{-1} = \{0, \ldots, N_T - 1\}$ be the set of discrete time steps and time steps except for the last, respectively. An aircraft is assumed to be a point mass operating in two-dimensional airspace, meaning that the vehicle maintains the same altitude during the cruise segment. The position of aircraft at a specific time step t is defined by (x_t, y_t), forming the position vector $\boldsymbol{r}_t = (x_t, y_t)^\mathsf{T}$. The velocity and acceleration of aircraft are specified in the vector form $\boldsymbol{v}_t = (v_{x_t}, v_{y_t})^\mathsf{T}$ and $\boldsymbol{a}_t = (a_{x_t}, a_{y_t})^\mathsf{T}$, respectively.

Constraint: Departure from Origin and Discrete Vehicle Dynamics

The departure location of aircraft is specified as

$$\boldsymbol{r}_{t_{\text{dep}}} = \boldsymbol{r}^{I}, \tag{2}$$

where t_{dep} is the time step where the aircraft plans to depart at the origin, and $\boldsymbol{r}^{I} = [x^{I}, y^{I}]^{\mathsf{T}}$ is the departure position vector of the vehicle in the $x-$ and $y-$axes. The discretized dynamics of the point mass are detailed such that

$$\boldsymbol{r}_{t+1} = \boldsymbol{r}_t + \Delta t \boldsymbol{v}_t + \frac{(\Delta t)^2}{2}\boldsymbol{a}_t, \qquad \forall t \in \mathcal{T}^{-1} \tag{3a}$$

$$\boldsymbol{v}_{t+1} = \boldsymbol{v}_t + \Delta t \boldsymbol{a}_t. \qquad \forall t \in \mathcal{T}^{-1} \tag{3b}$$

Constraint: Maximum Velocity and Acceleration

The aerial vehicle is subject to magnitude limits of velocity and acceleration. The exact mathematical formulation of the maximum velocity and acceleration is

$$v_{x_t}^2 + v_{y_t}^2 \leq V_{\max}^2,$$
$$a_{x_t}^2 + a_{y_t}^2 \leq a_{\max}^2,$$

where each represents a non-linear circle shape, and $V_{\max}$ and $a_{\max}$ are the maximum velocity and acceleration that the vehicle could have, respectively. These representations can be approximated by using a large number of linear inequalities, i.e., producing m-sided polygons in sets of $\mathcal{T}$ and $\mathcal{M}$ such that

$$v_{x_t} \sin\left(\frac{2\pi m}{N_M}\right) + v_{y_t} \cos\left(\frac{2\pi m}{N_M}\right) \leq V_{\max} e_t, \qquad \forall t \in \mathcal{T},\ \forall m \in \mathcal{M} \tag{4a}$$

$$a_{x_t} \sin\left(\frac{2\pi m}{N_M}\right) + a_{y_t} \cos\left(\frac{2\pi m}{N_M}\right) \leq a_{\max} e_t, \qquad \forall t \in \mathcal{T},\ \forall m \in \mathcal{M} \tag{4b}$$

where $\mathcal{M} = \{0, \ldots, N_M\}$ is a set of m-sided polygons with the number of linear inequalities N_M. Note that when the number of linear inequalities more than 56, i.e., $N_M \geq 56$, is used to approximate a circle, it is known that the circumference of the polygon approximates that of the unit circle with little difference less than 0.01; thus, this research utilizes $N_M = 56$ to approximate the quadratic form of magnitude limit constraint closely. The binary variable e_t, indicating that the aircraft is airborne, 1, or on the ground, 0, at time step t, is introduced to set the velocity and acceleration values to zero when the vehicles are on the ground after landing.

Constraint: Arrival at Destination

The aircraft must arrive at the destination at a specific time step t before the time horizon T is ended. A binary variable d_t, which has either a value of 1 if the vehicle reaches the destination or 0 otherwise at time step t, is defined. The constraint of the destination arrival can be written as

$$|x_t - x^F| \leq R(1 - d_t), \qquad \forall t \in \mathcal{T},$$
$$|y_t - y^F| \leq R(1 - d_t), \qquad \forall t \in \mathcal{T},$$

in which absolute values can be expressed such that

$$\begin{aligned} x_t - x^F &\leq R(1 - d_t), \qquad \forall t \in \mathcal{T} \\ x^F - x_t &\leq R(1 - d_t), \qquad \forall t \in \mathcal{T} \\ y_t - y^F &\leq R(1 - d_t), \qquad \forall t \in \mathcal{T} \\ y^F - y_t &\leq R(1 - d_t), \qquad \forall t \in \mathcal{T} \end{aligned} \tag{5a}$$

$$\sum_{t=0}^{N_T} d_t = 1, \tag{5b}$$

where R is a sufficiently large number that should be larger than any other distance used in simulation, and x^F and y^F are an arrival location in $x-$ and $y-$axes, respectively. Eq. 5a describes that the aircraft position is aligned with the destination when the binary variable d_t is set to one, and Eq. 5b represents that the aircraft landing occurs only once.

Constraint: Aircraft on the Ground After Landing

The mathematical formulations of Eqs. 5a and 5b do not restrain the aircraft movement after landing, i.e., they allow the vehicle to be in motion even after the destination is reached at a specific time step t. To handle the issue, a binary variable f_t, implying at what time step the aircraft takes off, is defined and is coupled with the binary variables e_t and d_t such that

$$f_{t_{\text{dep}}} = 1, \tag{6a}$$

$$\sum_{t=0}^{N_T} f_t = 1, \tag{6b}$$

$$e_t = \sum_{l=0}^{t} (f_l - d_l)\,. \quad \forall t \in \mathcal{T} \tag{6c}$$

Eq. 6a represents that the binary variable f_t becomes one only at the scheduled departure time step t_{dep} and otherwise, zero, as described in Eq. 6b. The binary variable e_t is allowed to be one during flight segments between departure and arrival in Eq. 6c.

Constraint: Obstacle Avoidance

In the context of the UAM operations, restricted airspace (i.e., no-fly zones), such as convective weather areas and high-altitude structures, can be deemed as obstacles and must be avoided for flight safety. For simplicity, the obstacles are assumed to be a rectangle where $(Z^L_{x,s}, Z^L_{y,s})$ is the lower-left vertex and $(Z^U_{x,s}, Z^U_{y,s})$ is the upper-right vertex of the sth obstacle. A binary variable n_{tsk} is introduced, which indicates whether aircraft intrudes into the sth restricted area in the kth direction of $+x$, $-x$, $+y$, $-y$ at a specific time step t. The avoidance constraint can then be written in sets of $\mathcal{T}$ and $\mathcal{S}$ such that

$$\begin{aligned}
x_t - Z^U_{x,s} &\geq -Rn_{ts1}, && \forall t \in \mathcal{T},\ \forall s \in \mathcal{S} \\
Z^L_{x,s} - x_t &\geq -Rn_{ts2}, && \forall t \in \mathcal{T},\ \forall s \in \mathcal{S} \\
y_t - Z^U_{y,s} &\geq -Rn_{ts3}, && \forall t \in \mathcal{T},\ \forall s \in \mathcal{S} \\
Z^L_{y,s} - y_t &\geq -Rn_{ts4}, && \forall t \in \mathcal{T},\ \forall s \in \mathcal{S} \qquad (7a) \\
\sum_{k=1}^{4} n_{tsk} &\leq 3, && \forall t \in \mathcal{T},\ \forall s \in \mathcal{S} \qquad (7b)
\end{aligned}$$

where $\mathcal{S} = \{1, \ldots, N_S\}$ is a set of obstacles and N_S is the number of obstacles. Eq. 7a represents that when the aircraft intrudes into the sth restricted area at a time step t, the four binary variables, n_{ts1}, n_{ts2}, n_{ts3}, and n_{ts4}, are set to ones making a sum of 4, which should be prohibited by Eq. 7b.

Constraint: Battery Energy Consumption

The battery energy state must be taken into account for eVTOL vehicles. Recalling the definition of SOC in Eq. 1, the SOC is utilized to evaluate how much battery level remains at a specific time after flight segments. The necessary constraints can be defined in sets of $\mathcal{T}^{-1}$ and $\mathcal{T}$ as

$$f_{t_{\text{dep}}} = SOC_{\text{full}}, \tag{8a}$$

$$f_{(t+1)} = f_t - SOC_{t,\text{used}}, \quad \forall t \in \mathcal{T}^{-1} \tag{8b}$$

$$f_t \geq SOC_{\text{limit}}, \quad \forall t \in \mathcal{T} \tag{8c}$$

where SOC_{full} is a full battery capacity, that is, 100%, $SOC_{t,\text{used}}$ is the energy state consumed until a time step t, and SOC_{limit} indicates the battery limit that the vehicle should not extract below to ensure battery health and flight safety.

Eq. 8a describes that the vehicle starts operation with a full battery capacity, and Eq. 8b indicates how much battery is used at each time step, which significantly varies depending on the flight segment. Finally, Eq. 8c does not allow the aircraft to operate below the SOC limit, which is set to 20% in this work.

Objective: Minimum Flight Time

The primary objective of trajectory optimization is often to have the shortest flight time. This is found by minimizing the time that the aircraft stays in the air and the time that it takes to reach the destination. The objective function is provided as

$$\min_{e,\,d} \quad J = \sum_{t=0}^{N_T} t(e_t + d_t). \tag{9}$$

B. ILP-based Diversion Decision-Making

The diversion decision support tool ranks alternate destinations depending on the scoring function along with contingency scenario type and then provides the best alternate destination. To this end, this research formulates the Integer Linear Programming (ILP), in which all objectives and constraints are linear with only discrete variables.

Constraint: Only One Selection of Alternate Destination

Among several candidates of reachable destinations, only one destination should be selected as

$$\sum_{i=1}^{N_D} \delta_i = 1, \tag{10}$$

where N_D is the number of reachable alternate destinations and δ_i is a binary variable that has either a value of 1 if ith reachable alternate destination is selected or 0 otherwise.

Objective: Minimum Flight and Recovery Time

Depending on off-nominal situations, the objective (i.e., scoring) function can be changed. For the case of original aerodrome disruptions, the aggregation time of UAM flight time and passenger recovery time by driving is minimized such that

$$\min_{\delta} \quad J = \sum_{i=1}^{N_D} (t_{\text{flt},i} + t_{\text{rec},i})\delta_i, \tag{11}$$

where $t_{\text{flt},i}$ and $t_{\text{rec},i}$ are time required to reach ith alternate destination from where the diversion is declared and time that it takes from ith alternate destination to original one by driving, respectively.

In the case of a medical emergency, the flight time is just minimized as

$$\min_{\delta} \quad J = \sum_{i=1}^{N_D} t_{\text{flt},i}\delta_i. \tag{12}$$

V. Application to Real-World Operational Scenarios

This section aims to demonstrate the capability of the proposed framework by applying the framework to real-world operational scenarios. The city of Miami is selected as the place of demonstration because the city may significantly benefit from an aerial mobility service to overcome the geographical challenges of some water-locked areas which currently rely on only bridges to access the North, Mid, and South beaches [26–28]. The following three operational scenarios are presented to prove various functionalities of the framework. Case study 1 features UAM normal operations where the vehicle operates at different cruise altitudes of 1,000 ft and 2,000 ft from the scheduled departure and arrival locations. Case study 2 features the UAM contingency planning to handle the first off-nominal scenario of a disruption at the original aerodrome, resulting in diversion to one of the reachable heliports. Case study 3 focuses on the contingency planning to address the second off-nominal scenario of in-flight medical emergency by rerouting to the nearby hospitals. The rest of this section describes how the simulation environment has been modeled to conduct the three case studies and the details of each case study.

A. Environment Modeling

Existing airports and heliports are utilized for the UAM take-off and landing in the various scenarios investigated. Each location is defined as a geographical position, i.e., latitude and longitude, and collected as a vector point format in a shapefile through the ArcGis Hub [29]. The shapefile contains names, positions, elevations, and type codes (airports, heliports, seaports, etc.) of aerodromes located across the United States. The high-altitude structures and their boundaries are gathered in vector polygons via the Miami-Dade County's Open Data Hub [30], which provides a variety of datasets and resources for research and policy development. The structure data includes a collection of large commercial, industrial, or other non-residential buildings with associated heights and areas. Lastly, hospitals are leveraged as diversion landing sites in case of an in-flight medical emergency. The hospital information, including positions, addresses, number of beds, and whether they have emergency rooms, are collected in a shapefile through the Miami-Dade County's Open Data Hub [31].

As the proposed framework sets a distinct bounding box in each scenario, the airports and heliports, structures, and hospitals within the region of interest are filtered. Additionally, the coordinate reference system of all data expressed in the World Geodetic System 1984 (i.e., WGS84) is converted to the North American Datum (NAD) 83 (i.e., East Florida Projection) to express the associated locations in meters. The data pre-processing for tall structures is required because a rectangular obstacle aligned in $x-$ and $y-$axes is mathematically formulated in Section IV.A. The boxes enclosing non-rectangular building polygons are generated, and a user-defined buffer distance is applied around the box to provide the vehicle with a safety margin, as shown in Figure 5.

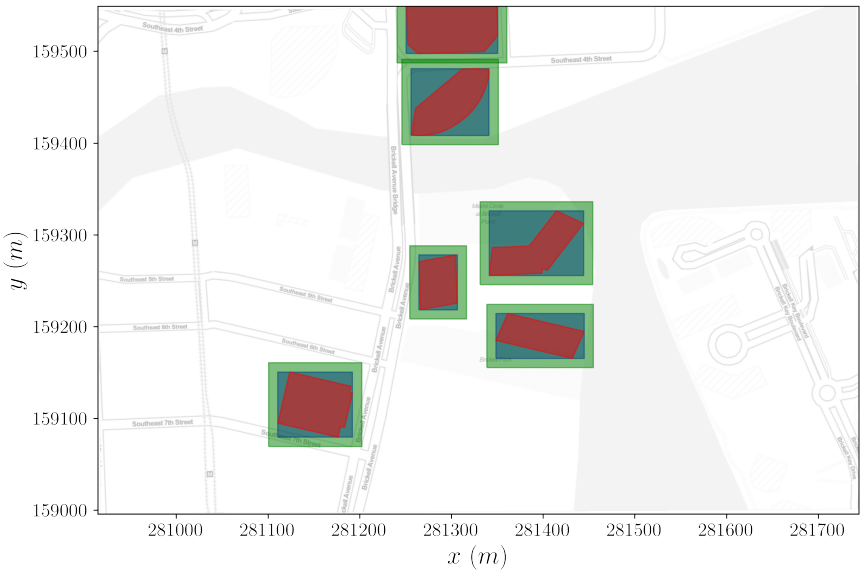

Fig. 5 Box enclosing non-rectangular structure polygons with safety buffer

B. Case Study 1: Normal Operation

The first case study demonstrates the capability of the proposed pre-flight planning system in the UAM normal operations. The following scenario is assumed. An UAM operator generates a flight plan between the origin at the Wharf Miami and the destination at South Pointe Park in the morning and another plan between the same locations in the afternoon, according to the flight schedule. Despite the same itinerary, different cruise altitudes are assigned to coordinate with other airspace participants. Figure 6 illustrates the trajectory differences for the two flight plans, which have the same departure and arrival locations yet different cruise altitudes, 1,000 ft and 2,000 ft. The 1,000 ft cruise flight detours the high-level structures with heights of more than 500 ft to avoid unexpected wind gusts. In contrast, the 2,000 ft cruise flight travels directly to the destination without encountering any turbulence because it flies at an altitude much higher than the tallest building. Table 2 describes time and battery energy which the eVTOL spent over each flight segment for the 1,000 ft and 2,000 ft flight plans. It is assumed that all segments except for climb, cruise, and descent have the same mission time, resulting in the identical energy consumption in both plans. With the additional assumption such that rate of climb and descent are $ROC_{\text{climb}} = 4\,\text{m/s}$ and $ROD_{\text{descent}} = -4\,\text{m/s}$, mission times over

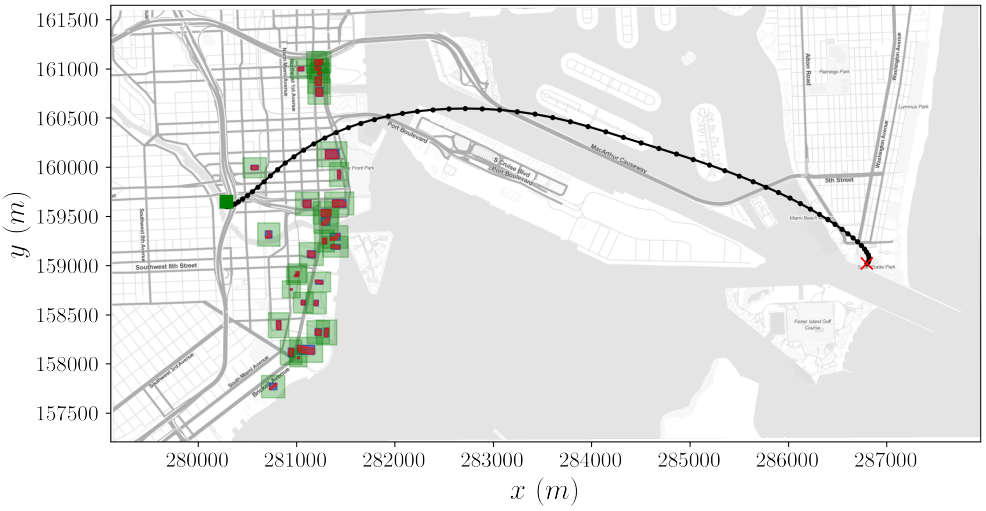

(a) 1,000 ft cruise altitude

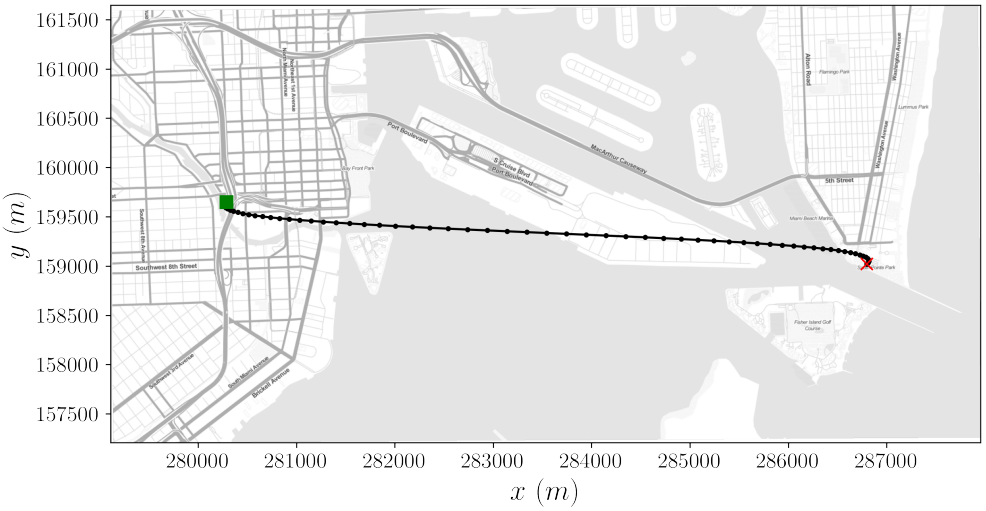

(b) 2,000 ft cruise altitude

Fig. 6 Flight trajectory changes with different cruise levels (green square: origin, red X: destination)

climb and descent segments are calculated as 61 s for 1,000 ft and 138 s for 2,000 ft cruise operations. It is noted that the cruising time of the vehicle operating at 1,000 ft is about 18 s longer than that operating at 2,000 ft due to taking a detour around the restricted tall buildings. Overall, an additional 136 s is spent in the 2,000 ft operation leading to more energy consumption 115.12 kWh and battery SOC 63.96% in comparison with the 1,000 ft operation which consumed slightly less at 109.15 kWh and 60.64%.

Table 2 Differences in mission time, energy consumption, and battery state for the UAM operating at two cruise altitudes 1,000 ft **and** 2,000 ft

Flight Segment	Cruise Altitude 1,000 ft			Cruise Altitude 2,000 ft		
	Time (s)	Energy (kWh)	Energy (%)	Time (s)	Energy (kWh)	Energy (%)
Taxi & Hover	30	9.14	5.08	30	9.14	5.08
Vertical Take-off	60	18.68	10.38	60	18.68	10.38
Transition Forward	45	17.83	9.91	45	17.83	9.91
Climb	61	4.39	2.44	138	9.93	5.52
Cruise	204	13.02	7.23	186	11.87	6.6
Descent	61	1.25	0.69	138	2.83	1.57
Transition Reverse	45	17.83	9.91	45	17.83	9.91
Vertical Landing	60	17.87	9.93	60	17.87	9.93
Hover & Taxi	30	9.14	5.08	30	9.14	5.08
Total/Available	596	180.00	100.00	732	180.00	100.00
Expended		**109.15**	**60.64**		**115.12**	**63.96**
Remaining		70.85	39.36		64.88	36.04

C. Case Study 2: Off-nominal Scenario of Aerodrome Disruption

The second case study is presented to demonstrate how the first off-nominal situation, mentioned in Section III.B.2, could be handled by the proposed contingency planning system. The following scenario is assumed. The pre-flight planning creates an initial flight plan which takes off at the Miami International Airport and arrives at the Miami Beach Convention Center. After a few minutes elapse after take-off, an onboard pilot is contacted by the PSU such that the planned aerodrome is closed due to an emergency. The pilot decides to divert and find which is the best diversion aerodrome.

Figure 7 shows an alternate destination selection process by the contingency planning system. A total of nine heliports within the region of interest are retrieved from an alternate destination database to accommodate the diversion presented in Figure 7(a). Then, multiple optimized trajectories from the position where the situation arises to reachable heliports are generated by the in-flight replanner, as shown in Figure 7(b). Note that the second heliport is excluded from the list of candidates as it is unreachable by the vehicle based on the remaining battery level. Table 3 summarizes the reachable and unreachable heliports that are ranked at the moment in which the contingency situation occurs. Among the eight candidates, the diversion decision tool selects the fourth heliport as the best diversion site, depicted as the blue trajectory in Figure 7(c), as it has the lowest scoring function value 15.95 min by summing up the two different times, flight time 4.7 min and recovery time 11.25 min evaluated using traffic information at 10:00 April 24th, 2022.

An additional study is conducted to identify whether the best selected alternate destination varies dependent on traffic information at different times. Table 4 shows a slight variation in recovery time evaluated at two different time periods, 10:00 and 18:00 April 24th, 2022, which is named as time A and time B, respectively. For example, the recovery time from the fourth heliport to the original destination by driving is increased from 11.25 min at time A to 11.42 min at time B as it may confront high traffic volumes in the road, while recovering from the fifth site is decreased from 11.15 min at time A to 11.02 min at time B with reduced traffic. This change results in the selection of the best alternate landing site to shift from the fourth to the fifth heliport, as shown by the green trajectory in Figure 7(c).

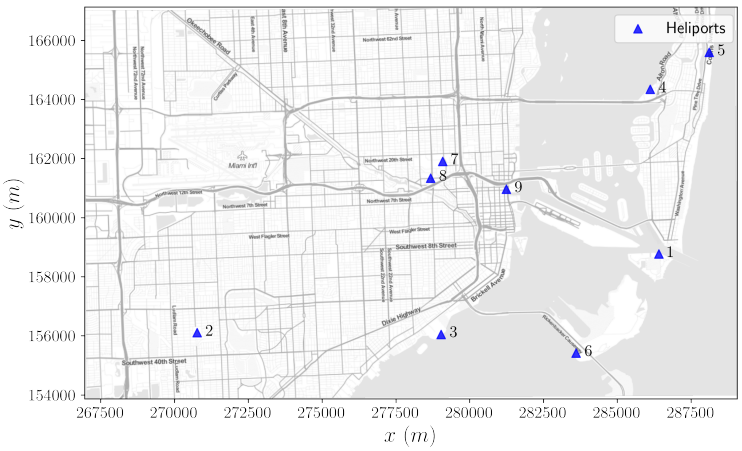

(a) Possible alternate heliports

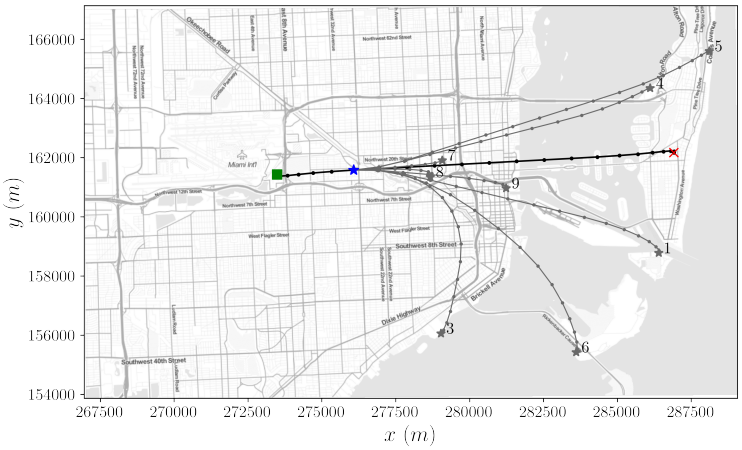

(b) Several optimal trajectories from contingency point to the reachable heliports

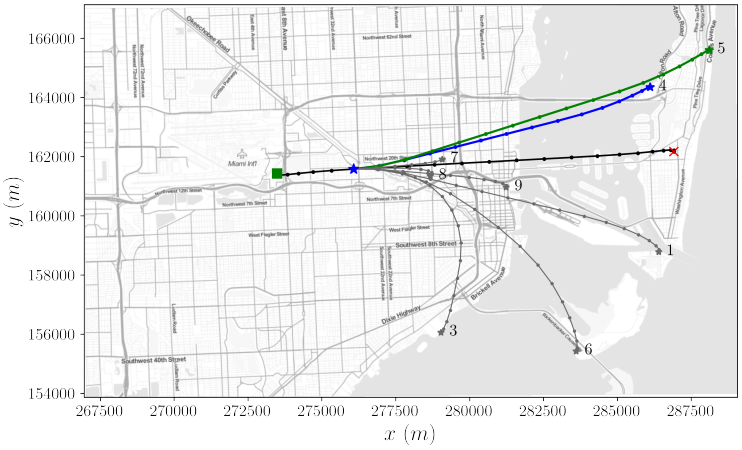

(c) Selection of the best heliport to divert

Fig. 7 Alternate destination selection procedure by the contingency planning system in case of a disruption at the original aerodrome (green square: origin, red X: scheduled destination, black line with dots: initial trajectory, blue star: contingency point, gray stars: reachable alternate heliports, blue and green lines with dots: two best alternate sites at different operation time)

Table 3 Ranked alternate heliports calculated at the moment that contingency situation arises

	Site Number	Remaining SOC (%)	Flight Time t_{flt} (min)	Recovery Time* t_{rec} (min)	Scoring Function $t_{\text{flt}} + t_{\text{rec}}$ (min)
Reachable Sites	4	22.69	4.7	11.25	**15.95**
	5	21.84	5.0	11.15	16.15
	9	25.24	3.4	17.05	20.45
	8	26.09	3.0	17.55	20.55
	7	26.09	3.0	17.77	20.77
	3	23.11	4.4	23.97	28.37
	6	23.11	4.4	25.7	30.10
	1	22.69	4.6	31.05	35.65
Unreachable Site	2	Below 20.00	·	·	·

* Recovery time is evaluated using traffic information at 10:00 April 24th, 2022

Table 4 Variation of recovery time and scoring values depending on traffic information at different time

Site Number	Flight Time (min)	10:00 April 24th, 2022		18:00 April 24th, 2022	
		Recovery Time (min)	Scoring Function (min)	Recovery Time (min)	Scoring Function (min)
1	4.6	31.05	35.65	31.83	36.43
3	4.4	23.97	28.37	23.67	28.07
4	4.7	11.25	**15.95**	11.42	16.12
5	5.0	11.15	16.15	11.02	**16.02**
6	4.4	25.7	30.10	25.47	29.87
7	3.0	17.77	20.77	17.82	20.82
8	3.0	17.55	20.55	17.32	20.32
9	3.4	17.05	20.45	16.72	20.12

D. Case Study 3: Off-nominal Scenario of In-flight Medical Emergency

The last case study is introduced to show how the proposed contingency planning system copes with the off-nominal situation of an in-flight medical emergency. While the UAM follows an initial optimal trajectory heading to the destination of the Bayfront Park from the origin of the Normandy Shores Golf Course, a passenger suddenly suffers a medical emergency in the air and must be escorted to a nearby hospital for urgent treatment. Figure 8 illustrates the best hospital selection process in case of a medical emergency. Figure 8(a) presents locations of hospitals equipped with emergency facilities, and Figure 8(b) shows several optimal trajectories connecting the contingency point to the reachable hospitals. It is noted that the third hospital is unreachable as the eVTOL no longer satisfies the SOC limit constraint to reach there. Table 5 summarizes the reachable and unreachable hospitals with remaining SOC and flight time. Out of ten reachable candidates, two hospitals, the eighth and ninth, are selected as the best diversion places as they all have the minimum flight time 4.05 min, as can be seen in Figure 8(c). It is important to mention that the diversion decision-making tool in this case, considers only the least flight time due to the nature of the urgent treatment.

Table 5 Ranked alternate hospitals estimated at the moment of medical emergency occurs

	Site Number	Remaining SOC (%)	Flight Time t_{flt} (min)
Reachable Sites	9	23.86	**4.05**
	8	23.86	**4.05**
	1	23.86	4.15
	4	23.54	4.20
	10	23.54	4.20
	11	22.58	4.65
	5	21.62	5.10
	2	21.31	5.25
	7	20.67	5.55
	6	20.35	5.70
Unreachable Site	3	Below 20.00	·

VI. Conclusion and Future Work

An automated framework composed of pre-flight and contingency planning systems was proposed. The pre-flight planning system uses a MILP-based planner to optimize a trajectory with the objective of minimum travel time between the scheduled origin and destination, avoiding restricted airspace, and tracking the consumed battery energy state. The contingency planning is made of two subsystems, the MILP-based in-flight replanner and the ILP-based diversion decision-making tool. The former generates the list of optimal trajectories from the contingency position to reachable alternate destinations that provide arrival time and battery energy estimates. The latter ranks candidates with the lowest scoring function values and returns the best site for diversion. The capability of the proposed framework was demonstrated by presenting three real-world operational scenarios. The first scenario was representative of flight planning in UAM normal operations, while the second and third scenarios featured cases of irregular operations. The results showed that the framework was not only capable of producing the optimal trajectory in the normal operation using pre-flight planning, but also successfully handled off-nominal situations using contingency planning. Despite the successful demonstration of the proposed framework, additional improvements will be investigated in future work. For instance, the framework applied for a single eVTOL UAM operation can be extended to multi-vehicle operations that ensure flight separation. Furthermore, non-rectangular obstacles could be mathematically formulated to increase the accuracy of flight time and energy estimates in the low-level urban airspace.

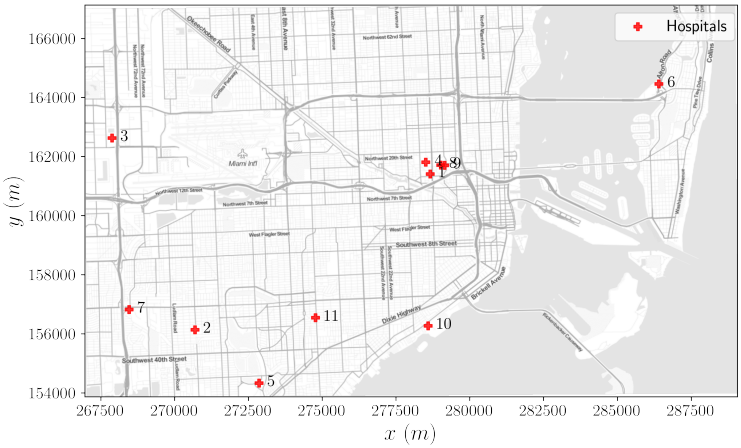

(a) Hospitals equipped with an emergency facility

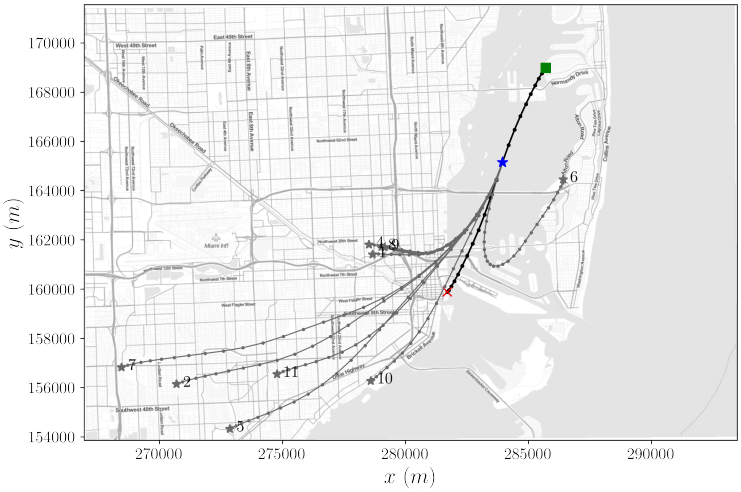

(b) Several optimal trajectories from contingency point to the reachable hospitals

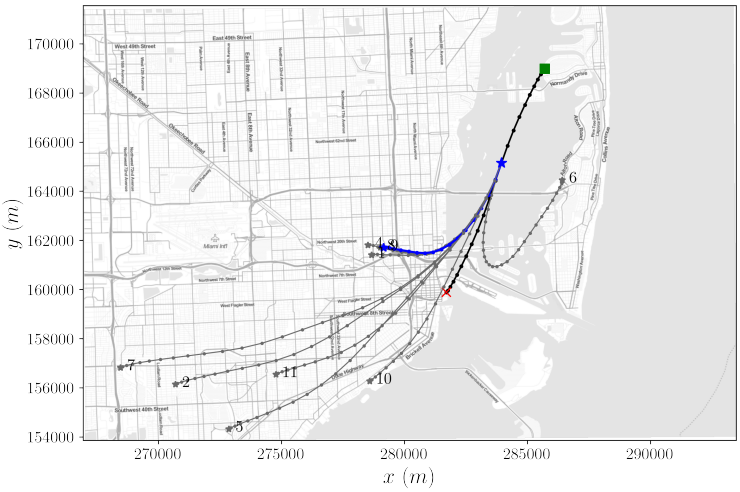

(c) Selection of the best hospital to divert

Fig. 8 Alternate destination selection process by the contingency planning system in case of in-flight medical emergency

References

[1] Goyal, R., Reiche, C., Fernando, C., Serrao, J., Kimmel, S., Cohen, A., and Shaheen, S., "Urban air mobility (UAM) market study," Tech. rep., 2018.

[2] Grandl, G., Ostgathe, M., Cachay, J., Doppler, S., Salib, J., and Ross, H., "The future of vertical mobility," *Porsche Consulting Study, Available online at https://www.porsche-consulting.com/us-en/press/insights/detail/study-the-future-of-vertical-mobility-1*, 2018 (Accessed April 8, 2022).

[3] Holden, J., and Goel, N., "Fast-forwarding to a future of on-demand urban air transportation," *Uber Elevate, Available online at https://evtol.news/__media/PDFs/UberElevateWhitePaperOct2016.pdf*, 2016 (Accessed April 8, 2022).

[4] Antcliff, K. R., Moore, M. D., and Goodrich, K. H., "Silicon valley as an early adopter for on-demand civil VTOL operations," *16th AIAA Aviation Technology, Integration, and Operations Conference*, 2016, p. 3466.

[5] Thipphavong, D. P., Apaza, R., Barmore, B., Battiste, V., Burian, B., Dao, Q., Feary, M., Go, S., Goodrich, K. H., Homola, J., et al., "Urban air mobility airspace integration concepts and considerations," *2018 Aviation Technology, Integration, and Operations Conference*, 2018, p. 3676.

[6] A3 by Airbus, "Blueprint for the Sky: The Roadmap for the Safe Integration of Autonomous Aircraft," *Available online at https://storage.googleapis.com/blueprint/Airbus_UTM_Blueprint.pdf*, 2018, (Accessed April 20, 2022).

[7] Boeing Next, "Flight Path for the Future of Mobility," *Available online at https://www.boeing.com/NeXt/common/docs/Boeing_Future_of_Mobility_White%20Paper.pdf*, (Accessed April 20, 2022).

[8] Tang, H., Zhang, Y., Mohmoodian, V., and Charkhgard, H., "Automated flight planning of high-density urban air mobility," *Transportation Research Part C: Emerging Technologies*, Vol. 131, 2021, p. 103324.

[9] Zhu, G., and Wei, P., "Pre-departure planning for urban air mobility flights with dynamic airspace reservation," *AIAA Aviation 2019 Forum*, 2019, p. 3519.

[10] Galway, D., Etele, J., and Fusina, G., "Modeling of the urban gust environment with application to autonomous flight," *AIAA Atmospheric Flight Mechanics Conference and Exhibit*, 2008, p. 6565.

[11] Raza, S. A., "Autonomous UAV control for low-altitude flight in an urban gust environment," Ph.D. thesis, Carleton University, 2015.

[12] Ayhan, B., Kwan, C., Budavari, B., Larkin, J., and Gribben, D., "Preflight contingency planning approach for fixed wing UAVs with engine failure in the presence of winds," *Sensors*, Vol. 19, No. 2, 2019, p. 227.

[13] The Vertical Flight Society, "eVTOL Aircraft Directory," *https://evtol.news/aircraft*, Accessed April 19, 2022.

[14] Stoll, A., "Analysis and Full Scale Testing of the Joby S4 Propulsion System," *Transformative Vertical Flight Workshop*, 2015. Accessed: 2022-03-23.

[15] The Vertical Flight Society, "Joby S4," *https://evtol.news/joby-s4*, Accessed April 19, 2022.

[16] Beedie, S. M., Harris, C. M., Verberne, J. A., Justin, C. Y., and Mavris, D., "Modeling Framework for Identification and Analysis of Key Metrics for Trajectory Energy Management of Electric Aircraft," *AIAA AVIATION 2021 FORUM*, 2021, p. 3171.

[17] Skuhersky, M., "A First-Principle Power and Energy Model for eVTOL Vehicles," Bachelor's thesis, Florida Institute of Technology, 2017.

[18] Choudhry, A., Moon, B., Patrikar, J., Samaras, C., and Scherer, S., "CVaR-based Flight Energy Risk Assessment for Multirotor UAVs using a Deep Energy Model," *2021 IEEE International Conference on Robotics and Automation (ICRA)*, IEEE, 2021, pp. 262–268.

[19] Bruhl, R., Fricke, H., and Schultz, M., "Air taxi flight performance modeling and application," *Proceedings of the 14th USA/Europe Air Traffic Management Research and Development Seminar (ATM2021)*, 2021.

[20] Kamal, A. M., and Ramirez-Serrano, A., "Design methodology for hybrid (VTOL+ Fixed Wing) unmanned aerial vehicles," *Aeronautics and Aerospace Open Access Journal*, Vol. 2, No. 3, 2018, pp. 165–176.

[21] Johnson, W., *Helicopter Theory*, Dover Books on Aeronautical Engineering Series, Dover Publications, 1994. URL https://books.google.com/books?id=SgZheyNeXJIC.

[22] Johnson, W., Silva, C., and Solis, E., "Concept vehicles for VTOL air taxi operations," *AHS Specialists"Conference on Aeromechanics Design for Transformative Vertical Flight*, 2018.

[23] Microsoft, "Bing Maps Routes API," *Available online at https://docs.microsoft.com/en-us/bingmaps/rest-services/routes/*, 2020 (Accessed April 20, 2022).

[24] Richards, A. G., "Trajectory optimization using mixed-integer linear programming," Ph.D. thesis, Massachusetts Institute of Technology, 2002.

[25] Culligan, K. F., "Online trajectory planning for UAVs using mixed integer linear programming," Ph.D. thesis, Massachusetts Institute of Technology, 2006.

[26] Eve Mobility, "Embraer's Eve Consortium Announces Initial Urban Air Mobility Concept of Operations in Miami-Dade County," *Available online at https://eveairmobility.com/embraers-eve-consortium-announces-initial-urban-air-mobility-concept-of-operations-in-miami-dade-county/*, 2022 (Accessed April 20, 2022).

[27] Archer, "Archer Announces Commitment to Launching its Urban Air Mobility Network in Miami by 2024," *Available online at https://www.archer.com/news/archer-taps-fcas-scale-and-expertise-to-accelerate-electric-vertical-take-off-and-landing-aircraft-evtol-production11*, 2021 (Accessed April 20, 2022).

[28] Supernal, "Supernal and City of Miami Agree to Enable Development of Advanced Air Mobility," *Available online at https://newsroom.supernal.aero/supernal-and-city-of-miami-agree-to-enable-development-of-advanced-air-mobility-143ae88cf466*, 2022 (Accessed April 20, 2022).

[29] Federal Aviation Administration, "Airport data," *ArcGIS Hub, Available online at https://hub.arcgis.com/documents/f74df2ed82ba4440a2059e8dc2ec9a5d/explore*, 2022 (Accessed April 20, 2022).

[30] Miami-Dade County, "Large building data," *Miami-Dade County Open Data Hub, Available online at https://gis-mdc.opendata.arcgis.com/datasets/MDC::large-building/explore?location=25.604674%2C-80.498549%2C10.78*, 2019 (Accessed April 20, 2022).

[31] Miami-Dade County, "Hospitals," *Miami-Dade County Open Data Hub, Available online at https://gis-mdc.opendata.arcgis.com/datasets/MDC::hospital/about*, 2018 (Accessed April 20, 2022).